Journal of Building Engineering 128 (2026) 116642

Contents lists available at ScienceDirect

Journal of Building Engineering

journal homepage: www.elsevier.com/locate/jobe

Fast characterization of wall thermal performance via enhanced hot box methodology

Maja Danovska *, Davide Cassol, Ivan Giongo, Alessandro Prada

University of Trento, Department of Civil Environmental and Mechanical Engineering, Via Mesiano 77, Trento, 38123, Italy

A B S T R A C T

Accurate thermal characterization of building envelope components is essential for energy-efficient and climate-resilient design. Conventional hot-box testing requires separate and prolonged procedures to determine steady-state (U-value) and periodic thermal properties, resulting in high experimental time and energy demand. This study proposes an enhanced hot-box methodology combining two sequential tests within a single campaign: a first response-factor-based dynamic test using triangular temperature excitation to determine the U-value without full steady-state convergence, and then, a sinusoidal periodic test to identify thermal transmittance, decrement factor, and time shift. The procedure was validated on a lightweight insulated wall and a high-inertia masonry wall. Uncertainty propagation and optimization of excitation parameters were considered. Under optimized configurations, the dynamic method determined the U-value within ±4.0% of the steady-state reference for both wall typologies, while reducing testing time by up to 50% and energy consumption by up to 34%. For the massive wall, accurate results required careful tuning of excitation amplitude and test duration to avoid response truncation. Periodic thermal parameters were successfully identified and showed limited sensitivity to measurement noise. The proposed sequential framework enables integrated evaluation of steady-state and periodic properties with reduced experimental load. The method is reliable under controlled boundary conditions and appropriately selected excitation parameters, while high-inertia assemblies require careful tuning to ensure accuracy.

Nomenclature

Symbols		
A	*Semi-amplitude of the outdoor air's temperature signal*	[°C]
(a_1, …, a_4)	*Fitting functions' coefficients for heat flux at non-excited side*	
B	*Semi-amplitude of the internal heat flux signal*	[W m^{-2}]
(b_1, …, b_7)	*Fitting functions' coefficients for heat flux at excited side*	
c	*Specific heat*	[J kg^{-1} K^{-1}]
CLT	*Cross-laminated Timber*	
ΔT	*Temperature difference*	[K]
$\Delta\tau_{ie}$	*Time shift*	[h]
ε	*Hemispherical emissivity*	[−]
$\varepsilon_{\Delta T}$	*Expanded uncertainty related to the temperature difference*	[K]
EPS	*Extruded polystyrene*	
ε_{q_i}	*Expanded uncertainty related to the surface heat flux*	[W m^{-2}]
f	*Decrement factor*	[−]
ϕ	*Phase of the outdoor air's temperature function*	[rad]
h	*Heat transfer coefficient*	[W m^{-2} K^{-1}]
h_c	*Convective heat transfer coefficient*	[W m^{-2} K^{-1}]

(*continued on next page*)

* Corresponding author.
E-mail addresses: maja.danovska@unitn.it, maja.danovska@hotmail.it (M. Danovska).

https://doi.org/10.1016/j.jobe.2026.116642
Received 10 December 2025; Received in revised form 13 March 2026; Accepted 13 June 2026
Available online 16 June 2026
2352-7102/© 2026 The Authors. Published by Elsevier Ltd. This is an open access article under the CC BY license (http://creativecommons.org/licenses/by/4.0/).

(*continued*)

Symbols		
h_r	*Radiative heat transfer coefficient*	[W m^{-2} K^{-1}]
L	*Wall's thickness*	[m]
λ	*Thermal conductivity*	[W m^{-1} K^{-1}]
N	*Duration of the test*	[min]
ω	*Angular frequency*	[rad s^{-1}]
P	*Period*	[s]
ψ	*Phase of the internal heat flux function*	[rad]
q_0	*Boundary heat flux*	[W m^{-2}]
$\dot{q}$	*Heat flux*	[W m^{-2}]
PUR	*Polyurethane*	
ρ	*Specific Mass*	[kg m^{-3}]
σ	*Stefan-Boltzmann constant*	[W m^{-2} K^{-4}]
t	*Time (dynamic test)*	[h]
τ	*Time (periodic function)*	[s]
T	*Temperature*	[°C]
U	*Steady-state thermal transmittance*	[W m^{-2} K^{-1}]
$U_{dyn,X}$	*Dynamic thermal transmittance calculated with heat flux data at the excited side*	[W m^{-2} K^{-1}]
$U_{dyn,Y}$	*Dynamic thermal transmittance calculated with heat flux data at the non-excited side*	[W m^{-2} K^{-1}]
u_U	*Propagated uncertainty of the steady-state thermal transmittance*	[W m^{-2} K^{-1}]
u_{Udyn}	*Propagated uncertainty of the dynamic thermal transmittance*	[W m^{-2} K^{-1}]
v	*Air's velocity*	[m s^{-1}]
x	*Space coordinate*	[m]
Y_{ie}	*Periodic thermal transmittance*	[W m^{-2} K^{-1}]

Subscripts	
e	External air
exc	Excited side
FFT	Fast Fourier Transform
i	Internal air
non-exc	Non-excited side

1. Introduction

The building energy efficiency is a key aspect of the energy transition, as the building sector accounts for 28% of total energy use [1]. Within this sector, HVAC systems are the primary most energy-intensive components, responsible for approximately 25% of total demand [2]. The European directive EPBD IV [3] set minimum requirements to promote energy efficiency in buildings, aiming for a fully decarbonized building stock with low emissions by 2050. The building envelope significantly influences energy performance by regulating energy fluxes. Thermal transmittance, also known as U-value, is crucial, as it impacts heat losses, especially in winter. Such parameter depends on geometry, boundary conditions, and material thermal conductivity. However, as building components rarely operate under steady-state conditions, their dynamic thermal properties are essential, especially in hot seasons [4] and for buildings with massive envelope components [5]. A well-designed envelope can store and release heat efficiently, optimizing HVAC control strategies and enhancing energy flexibility, operating as a storage system [6,7]. Moreover, improved envelope design improves building resilience, mitigating heat transfer during heat waves.

There are different methods for determining thermal parameters of opaque components. For simple and homogeneous geometries, heat flux is considered as one-dimensional, allowing for a direct U-value assessment [8] through the electrical analogy method which depends on layer thickness, thermal conductivity, and boundary conditions. On the contrary, periodic thermal properties are usually calculated analytically according to the standard EN ISO 13786 [9]. However, standard methods may lack accuracy due to real walls' geometric inhomogeneities and material moisture content, affecting declared thermal properties which are adopted inside the analytical method [10]. Wrong assumptions can result in erroneous thermal parameter estimations [11] and discrepancies in thermal performance predictions [12,13]. Hence, direct measurement methods are preferred for a greater accuracy in thermal characterization. Laboratory hot-box methods allow for controlled boundary conditions [14,15]. Nevertheless, they are extremely time-consuming and energy intensive tests, especially for components characterized by high thermal capacitance. While a clear legislative framework exists for U-value determination [16,17], and a well-established procedure is extensively used [18], periodic thermal parameter assessment lacks a standardized methodology. Some studies [4,19,20] have replicated sinusoidal temperature variations using modified hot-box setups with external heating, while in Ref. [5] authors have experimented with periodic properties via calibrated hot-box systems. Additionally, dynamic test procedures based on response factors theory [14,21,22] have also been explored, applying impulsive temperature changes to determine wall thermal response [23–30]. In recent years, increasing attention has been devoted to the development of accelerated and non-steady experimental frameworks for wall thermal characterization. Transient hot-box investigations have demonstrated the feasibility of imposing sinusoidal or impulsive boundary conditions to experimentally derive periodic thermal parameters under controlled laboratory settings [19]. Other recent works have explored modified hot-box or transient methodologies aimed at reducing testing duration while maintaining acceptable accuracy in thermal parameter estimation [31,32]. These contributions highlight a growing interest in dynamic and non-destructive characterization strategies as alternatives to prolonged steady-state procedures. However, in most of these studies, steady-state, periodic, and response-factor-based tests are treated as separate experimental approaches. Periodic investigations generally rely on standard harmonic formulations (e.g., EN ISO 13786) to interpret stabilized sinusoidal responses, without explicitly reporting a direct measurement-based analytical link between the raw hot-box signals and the resulting thermal parameters within a unified workflow [19]. Similarly, response-factor-based dynamic tests have been mainly adopted for the determination of in-situ U-values of opaque components with the aim of overcoming unstable boundary conditions in real building tests and few works exploit triangular excitations only for retrieving response factor series of the tested opaque components [14]. Tests based on response factor theory are generally applied as stand-alone dynamic characterizations and are not explicitly integrated into a hot-box protocol aimed at determining both the U-value and periodic thermal properties within the same experimental campaign. Despite the hot-box reliability, no single methodology fully determines both static and periodic thermal characteristics. Tests are typically performed separately and are time intensive. Dynamic characterization, including the thermal inertia, shows promising outcomes but requires a broader application to a greater variety of wall types with different thermal resistance and inertia [22]. In fact, the systematic integration of transient U-value determination and periodic parameter extraction within a single structured hot-box protocol remains limited in the literature; however, such an optimized procedure could significantly reduce testing time while also decreasing the energy required during the experiments, thereby lowering operational costs.

Standardized procedures for guarded hot-box testing do not prescribe a fixed testing duration; however, steady-state measurements require the fulfilment of convergence and stabilization criteria before reliable thermal transmittance values can be obtained. For wall assemblies with high thermal inertia, the characteristic thermal response time can be significant, often leading to extended experimental durations before steady conditions are reached. Although specific test durations are rarely reported in the literature, it is widely recognized that massive wall systems require prolonged stabilization due to their high thermal capacitance.

The present work advances beyond this fragmented framework by proposing a sequenced experimental protocol that integrates a transient response-factor segment for U-value determination with a periodic excitation segment for the periodic thermal characterization within a single hot-box campaign. This study proposes a comprehensive experimental framework for fully characterizing steady-state and periodic thermal properties of walls through the complementary coupling of two hot-box test procedures. The methodology involved two main steps: a numerical model for simulated tests and an experimental phase. The simulated test is used to optimize the parameters to be employed during the experiment, considering the wall characteristics, the measurement accuracy and the constraints such as the signal-to-noise ratio. Following the simulated test, an experimental test is conducted using optimal parameters, selected according to the technical characteristics of the wall to improve the measurement accuracy as well as the time and energy required for the experiment. The experimental tests were carried out using a hot-box facility at the Sustainable Energy Laboratory, University of Trento. The U-value was determined via a first segment based on the response-factors theory without requiring full steady-state convergence and compared with the standard steady-state method. Immediately after the first segment, a second one is carried out to compute periodic thermal transmittance, decrement factor, and time lag exploiting a sinusoidal temperature solicitation test and a clear experimental link between measured signals and periodic thermal parameters. This research aims to suggest an efficient and standard experimental workflow for simultaneously assessing steady-state and periodic thermal properties, facilitating improved thermal envelope design for energy-efficient and climate-resilient buildings. The originality of the proposed framework lies in the integrated and optimized use of an impulse-based response-factor test and a subsequent periodic test within the same hot-box campaign, allowing a quantitative reduction of testing time and energy consumption, which has not been explicitly investigated in previous hot-box studies. The objective is not to define universal reductions in testing duration, but rather to provide a structured comparison between conventional steady-state procedures and the proposed two-segment approach under identical laboratory conditions. This framework enables the reduction in testing time and the associated energy demand to be quantitatively assessed within the same experimental setup. Two walls with distinct thermal resistance and inertia were tested: (1) an insulated wall with

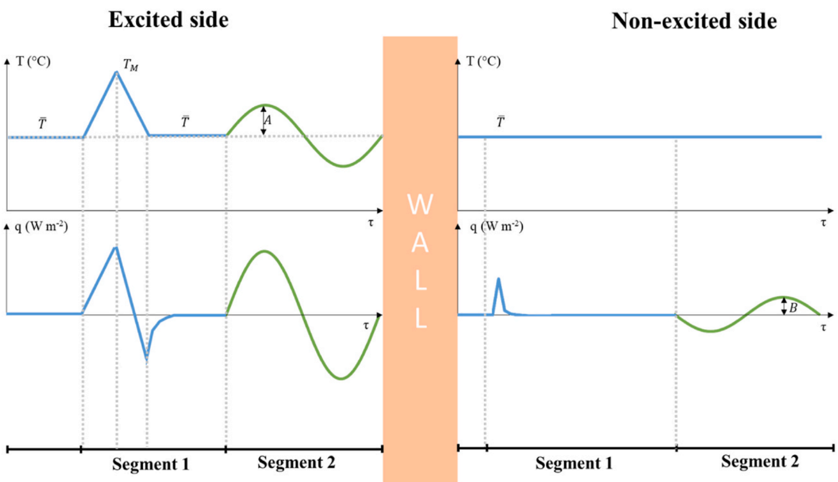

Fig. 1. Scheme of the boundary conditions during the test.

polyurethane and expanded polystyrene layers and (2) a masonry wall with solid bricks and a cross-laminated structural layer, featuring lower resistance but higher inertia.

2. Materials and methods

The procedure for the complete characterization of the energy performance of building envelope components consists of a test in a hot-box apparatus with two segments. The first segment is based on the response-factors theory. A triangular temperature solicitation is imposed with the aim of determining both the wall response factors and the U-value. Subsequently, the periodic thermal transmittance and the time shift, are determined through a second segment conducted under a periodic sinusoidal boundary condition. This procedure thus allows for the evaluation of the U-value, which is primarily used in calculating a building's heating load, along with the dynamic parameters employed in assessing cooling loads or in performing dynamic building simulations. Following sections provide a detailed description of the two test segments, as schematized in Fig. 1, and the required post-processing analyses.

2.1. *Segment 1: the response factors method*

The Response Factors method (RF) is an analytical approach used to model the transient thermal behaviour of multilayer walls under time-varying boundary conditions. RF estimates the transient response as a function of past temperatures and coefficients, defined response factors that are the heat fluxes caused by a unitary temperature pulse. Hence the superposition principle is used for simulating daily temperature changes and heat propagation through layered wall assemblies.

A dynamic test based on the response factor theory is performed to characterize the U-value of the wall. The test is initiated starting from homogeneous initial conditions of the sample at a temperature equal to $\overline{T}$. Hence, the two chambers of the hot box apparatus are conditioned at the same air's temperature equal to $\overline{T}$ to have a homogenous initial condition. After steady-state conditions are reached, the air temperature on the external side is varied according to a triangular function with a duration of 2 h. This triangular temperature variation was applied as a time-dependent boundary condition, with the time base for the response factors set to 1 h and maximum temperature of T_M. Following the pulse, the air temperature was returned to $\overline{T}$ and maintained for a sufficient duration, typically 24 h or more, depending on the specimen characteristics. Although the impulse should ideally be unitary, this would result in very low heat fluxes on the opposite side of the wall, which results in a very low signal-to-noise ratio. To increase measurement accuracy, the magnitude of the triangular ramp is determined based on the thermal characteristics, such as thermal resistance, of the wall. After that, measured values are consequently normalized with respect to the magnitude of the applied temperature profile magnitude. However, the choice of the pulse magnitude may undermine the linearity assumptions required to apply the superposition principle. In fact, an excessive temperature increase on the excited side may trigger local phenomena, such as enhanced radiative heat exchange within the cavities of porous materials or moisture migration, which can locally alter the apparent thermal conductivity. For this reason, the selection of T_M must balance the need for increasing the heat flux on the opposite side with the need to limit local disturbances related to the material properties.

Temperatures at the surfaces and heat fluxes are measured and post-processed to compute the thermal transmittance considering either the external (excited) and the internal (non-excited) heat fluxes. Since experimental data are subjected to noise during experimental tests, heat fluxes are firstly fit with two analytical functions. The one fitting the heat flux measured at non-excited side is reported in Eq. (1).

$$\dot{q} = a_1 \cdot e^{-a_2 \cdot \ln \frac{t}{a_3}^2} + a_4 \tag{1}$$

The heat flux at the excited side is fitted with a piece-wise function in three portions of the domain, as shown in Eq. (2):

$$\dot{q} = \begin{cases} b_1 \cdot e^{b_2 \cdot t} + b_3, 0 < t \leq 1 \\ b_1 \cdot e^{b_2} + b_3 - (b_1 - b_4) \cdot \left(1 - e^{b_5 \cdot (t-1)}\right), 1 < t \leq 2 \\ b_4 \cdot e^{b_6 \cdot (t-2) + b_7 \cdot (t-2)^{0.25}} + b_3 \; t > 2 \end{cases} \tag{2}$$

where the variable $\dot{q}$ refers to the heat flux measured every minute, (a_1, …, a_4) and (b_1, …, b_7) are the parameters of the fitting curves obtained by minimizing the root mean square error between the experimental data and the fitting curve and t is the time coordinate expressed in hours.

The U-value is calculated by summing separately heat flux values of the fitting curve every minute over the whole test time and dividing the result by the temperature magnitude (unitary signal) and a conversion factor equal to 60 to pass from minutes to hours. Two values of U can be obtained by summing the flux measured on the excited side (Eq. (3)) or on the non-excited side (Eq. (4)).

$$U_{dyn,X} = \sum_0^N X_i = \frac{\left(\sum_0^N \dot{q}_{exc}\right) - b_3}{60 \cdot \theta} \tag{3}$$

$$U_{dyn,Y} = \sum_0^N Y_i = \frac{\left(\sum_0^N \dot{q}_{non-exc}\right) - a_4}{60 \cdot \theta} \tag{4}$$

Indices of the summation refer to the number of heat flux terms to sum. The initial index is equal to zero, i.e. the time at which the temperature peak occurs on the excited side. N is equal to the test duration, usually occurring when the non-excited heat flux approaches zero after the excitation.

2.2. Segment 2: periodic thermal properties

In the second segment of the test, a stabilized periodic regime is maintained to measure the periodic thermal properties of the wall. After segment 1, the sample is in equilibrium at the initial temperature $\overline{T}$. Then, the temperature in the climatic chamber emulating the external environment is forced to follow a 24 h sinusoidal profile with an average temperature of $\overline{T}$ and semi-amplitude of A, while the other chamber is kept constant at $\overline{T}$. Once both temperatures and heat fluxes have reached the periodic steady-state condition, data is used to compute the periodic thermal transmittance (Y_{ie}), the decrement factor (f) and the time shift ($\Delta\tau_{ie}$). While the definitions of periodic thermal transmittance, decrement factor, and time shift are provided in the standard EN ISO 13786, the standard does not prescribe a measurement-based procedure for deriving these quantities directly from experimental data coming from hot-box apparatuses. In this work, a signal-processing formulation is therefore established to link the measured air temperature and heat-flux signals to the corresponding periodic thermal parameters. The procedure is based on harmonic decomposition of experimental data and on the explicit formulation of the complex amplitudes required to compute the periodic properties under controlled boundary conditions. To improve measurement accuracy, the signal is initially filtered to remove noise. The Fast Fourier Transform algorithm [33,34] is applied to the original data and only the fundamental harmonic is kept. Then measurements are postprocessed according to the theory of signals. The air temperature at the excited side and the heat flux on the non-excited side can be expressed as cosine functions with different phases, as seen in Eq. (5) and Eq. (6).

$$\mathrm{T_e}(x,\tau)|_{x=0} = A\cos(\omega\tau - \phi) \tag{5}$$

$$\dot{q}_i(x,\tau)|_{x=L} = B\cos(\omega\tau - \psi) \tag{6}$$

where $\omega = \frac{2\pi}{P}$ is the angular velocity expressed in (rad s^{-1}) and P the period in (s);

A and B denote the semi-amplitude of temperature and heat flux, respectively;

ϕ and ψ are the phase of the external air's temperature and the internal heat flux, respectively;

L is the total thickness of the tested wall and represents the space coordinate of the internal surface.

Eqs. (7) and (8) can be obtained by exploiting Euler's formula and taking just the real part [35].

$$\widetilde{T}_e(x,\tau)|_{x=0} = Re\left[A\cdot e^{-i\phi}\cdot e^{i\omega\tau}\right] = Re\left[\widehat{T}_e\cdot e^{i\omega\tau}\right] \tag{7}$$

$$\widetilde{\dot{q}}_i(x,\tau)|_{x=L} = Re\left[B\cdot e^{-i\psi}\cdot e^{i\omega\tau}\right] = Re\left[\widehat{\dot{q}}_i\cdot e^{i\omega\tau}\right] \tag{8}$$

where $\widehat{T}_e$ and $\widehat{\dot{q}}_i$ are the complex amplitudes of the two functions. According to the technical standard [9], the periodic thermal transmittance Y_{ie} is defined as the ratio of the complex amplitude of the heat flux at the non-excited side over the complex amplitude of the air's temperature (Eq. (9)).

$$Y_{ie} = \frac{\widehat{\dot{q}}_i}{\widehat{T}_e} = \frac{B\cdot e^{-i\psi}}{A\cdot e^{-i\phi}} = \frac{B}{A}\cdot e^{i(\phi-\psi)} = \frac{B}{A}\cdot\ [\cos(\phi-\psi) + i\sin(\phi-\psi)] \tag{9}$$

Since the thermal transmittance is expressed as a complex number, it can be characterized by a modulus and an argument. Thus, by assessing the modulus of Eq. (9), the periodic thermal transmittance is shown in Eq. (10).

$$|Y_{ie}| = \frac{B}{A}\cdot\sqrt{\cos^2(\phi-\psi) + \sin^2(\phi-\psi)} = \frac{B}{A} \tag{10}$$

while, $\Delta\tau_{ie}$ is obtained by calculating the argument of Eq. (9).

$$\Delta\tau_{ie} = \arg(Y_{ie}) = \arctan\frac{\sin(\phi-\psi)}{\cos(\phi-\psi)} = \frac{\phi-\psi}{2\pi}\cdot 24 \tag{11}$$

The decrement factor is then calculated according to Eq. (12) which represents the ratio of the modulus of the periodic thermal transmittance over the steady-state thermal transmittance U.

$$f = \frac{|Y_{ie}|}{U} = \frac{B}{A\cdot U} \tag{12}$$

2.3. Description of validation test cases

Two test cases are analysed in the validation of the procedure (Fig. 1). These walls were chosen to represent different construction materials and thermal properties, enabling a broad analysis of the thermal performance.

The first wall, named lightweight wall (LW), is composed of non-homogeneous layers made of polyurethane and expanded polystyrene panels anchored together with screw heads, and both surfaces covered with an aluminium layer with a negligible thermal resistance. Wall's dimensions are 250 × 250 cm and thickness equal to 12 cm. This wall was chosen to represent an extreme scenario of lightweight walls with improved thermal insulation. The second one, called massive wall (MW), is composed of solid bricks arranged in the two-headed brick layout, with a 6 cm thick structural layer of cross-laminated timber (CLT) installed on the external side. A vapor barrier is placed between the masonry and CLT layer to protect the timber layer from moisture. Prior to testing, the masonry specimen was stored in the laboratory environment for an extended conditioning period to minimize moisture gradients associated with drying processes. In addition, the applied vapor barrier was intended to limit moisture migration across the masonry-timber interface. This configuration was selected in accordance with innovative strategies for improving the seismic performance in masonry buildings by exploiting timber [36]. Wall's dimensions are 100 cm × 120 cm x 31 cm. The massive sample was built in an insulated frame around it, to establish a guard ring and consequently a mono-dimensional heat flux across the tested wall. Both samples satisfy conditions prescribed by the standard EN ISO 1934 [17] to reduce lateral heat fluxes. Two portions of the total surface were identified on both internal and external surfaces. A *measuring section*, with dimensions of 30 cm × 30 cm, with the aim of measuring the main quantities like heat flux and the surface's temperature necessary for the calculations. A *guard area* is defined and placed around the measuring area necessary for the verification of the uniformities of temperature and heat fluxes. The measuring area for the lightweight wall was placed in the upper part of the sample composed only by PUR layers. While, for the massive wall, the measuring area was placed in the centre of the CLT layer (Fig. 2).

Thermal properties of the adopted materials were either measured or taken from the literature (Table 1). In the specific, the measured thermal conductivity was obtained with a Hot Disk® apparatus (Model: HOT DISK TPS 2500 S) and the material's density was obtained by measuring the volume of the sample as well as its weight with an electronic scale (Model: Mettler Toledo PS6001-S, accuracy: ±0.06 g).

2.4. *Simulated tests*

Simulated tests were performed to ensure that the proposed experimental framework is correctly designed, to identify any potential issues before performing laboratory experiments and to optimize the test duration. These preliminary simulations were limited to the wall heat transfer problem, while the climatic chambers were represented through design temperature profiles and convective boundary conditions, with heat transfer coefficients estimated from empirical correlations based on previous climatic chamber measurements where airflows within the chambers were measured. A finite element model was developed in COMSOL Multiphysics® [44]. A two-dimensional geometrical model reproduces inside the software the vertical cross-sections in Fig. 2. A two-dimensional (2D) model was necessary, as the considered wall assemblies are not spatially uniform and local heterogeneities could influence the transient thermal response. During the experiments, moisture-related effects are intentionally limited by pre-conditioning the masonry specimen, by installing a vapor barrier between masonry and timber layers, and by controlling the air conditions in both chambers to maintain similar absolute humidity levels. Under these conditions, moisture transport effects are minimised, and a heat-transfer-only model was considered sufficient for the intended analysis. Hence, the numerical model was restricted to heat transfer only and did not include coupled heat and moisture transport. The vapor barrier was not explicitly modelled in the numerical simulations due to its negligible impact on heat transfer. The boundary conditions for the two vertical surfaces, facing the internal and external environments, were specified. A Newton-Robin boundary conditions is set on the two vertical surfaces, hence defining the convective heat flux (Eq. (13)). This requires setting both the heat transfer coefficient and the air temperature.

$$q_0 = h \cdot (T_{AIR} - T_s) \tag{13}$$

where q_0 is the boundary heat flux, h denotes the heat transfer coefficient, T_{AIR} and T_s are respectively the air's temperature and the surface temperature on the wall. The quantities h_{int} and h_{ext} were calculated as a function of wind speed and air temperature according to the standard EN ISO 6946 [8], as shown in Eq. (14).

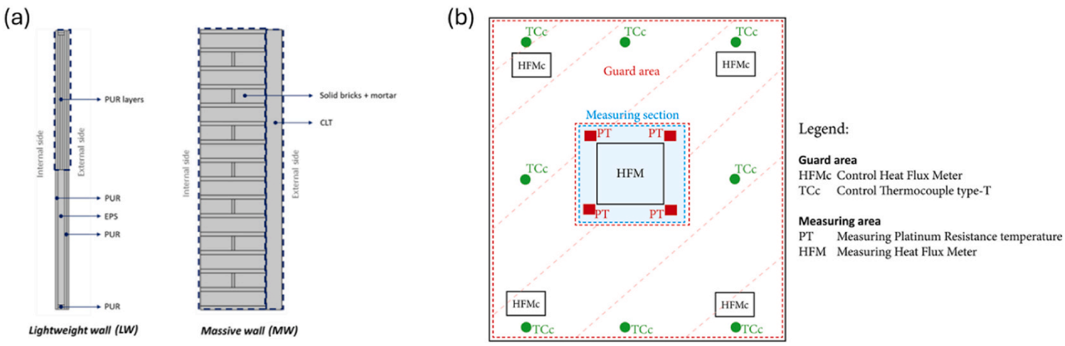

Fig. 2. Description of the analysed samples (vertical cross section) (a) and the layout of samples' surfaces, highlighting the measurement and the guard area (b).

Table 1
Thermo-physical properties of materials composing the analysed walls. Thermal conductivity uncertainty equal to ±3%, density uncertainty equal to ±5%.

Wall	Material	λ (W m^{-1} K^{-1})	ρ (kg m^{-3})	c (J kg^{-1} K^{-1})
LW	**EPS**	0.031 (measured)	19 (measured)	1340 [37]
	PUR	0.025 (measured)	49 (measured)	1100 [38]
MW	**Solid brick**	0.690 (measured)	1678 (measured)	850 [39]
	Mortar	0.850 (measured)	1370 [40]	900 [41]
	CLT	0.100 (measured)	420 [42]	1600 [43]

$$h = h_c + h_r = 4 + 4 \cdot v + \epsilon \cdot \sigma \cdot T_{mn}^3 \tag{14}$$

where h_c is the convective heat transfer coefficient due to the air speed adjacent set into the hot-box. h_r is the linearized radiative heat transfer coefficient obtained from the hemispherical emissivity of the surface, the Stefan-Boltzmann constant and the mean thermodynamic temperature of the surface. The two horizontal surfaces were set as adiabatic surfaces.

Time-dependent heat-transfer problems were solved using finite-element discretization with triangular elements and quadratic interpolation. A user-controlled mesh was adopted to accurately solve local temperature gradients across the multilayered structure. An explicit Runge-Kutta RK34 scheme was adopted, with a relative solver tolerance set to 10^{-4}. Numerical stability was ensured through adaptive time stepping, which automatically adjusted the internal time step to account for the diffusion-dominated nature of the problem and the adopted spatial discretization. A mesh sensitivity analysis was conducted for the two walls' typologies to quantify the extent to which outcomes are sensitive to geometry discretization. This involved conducting the tests while adjusting the mesh from a normal setting (with maximum size of 7.04 cm and minimum size of 0.03 cm) to an extremely fine setting (with maximum size of 1.05 cm and minimum size of 0.002 cm). Possible variations in results were carefully examined, and a discretization level was selected for all the analysis equal to normal.

The numerical model was therefore used to simulate the test involving the two segments, with the aim of identifying testing conditions that could reduce the duration of the experiments while simultaneously maintaining the signal-to-noise ratio requirements, which significantly affect measurement accuracy.

2.5. *Experimental tests*

An extensive experimental campaign was carried out at the Sustainable Energy Laboratory at the University of Trento to validate proposed methodology. Firstly, the test described in Sections 2.1 and 2.2. was performed. Following on from this point, a steady-state test was conducted with the aim of determining the reference U-value according to the standard EN ISO 1934 [17].

The hot-box apparatus, designed and constructed by Biemme di Marenghi G. & c. sas., features two glass-fibre insulated chambers (250 cm × 250 cm) for simulating indoor and outdoor conditions (Fig. 3). These chambers are mounted on rails and move via a powered rack-pinion system controlled by a panel. A fixed 70 cm-wide insulating frame between them hosts the tested sample ensuring minimal heat loss during operation. Each chamber includes an air-conditioning unit to maintain constant temperature and relative humidity.

Panel with low-emissivity coatings are installed near the sample in both zones to reduce and uniform radiative heat exchange, creating an air gap between the panel and the wall. Four and six axial fans in the indoor and outdoor chambers generate the airflow in the gap to prevent thermal stratification. Ambient conditions are controlled by PID regulators for temperature, humidity, and wind speed, managed via PC with LabVIEW software (RS 422 interface). Sensors include eight temperature probes (Platinum RTD), two humidity probes (capacity sensors), and two hot wire anemometers for the wind speed measure are installed and sampled every 30 s.

In contrast, the measurements used for the determination of performance parameters are collected using a dedicated data acquisition system, consisting of:

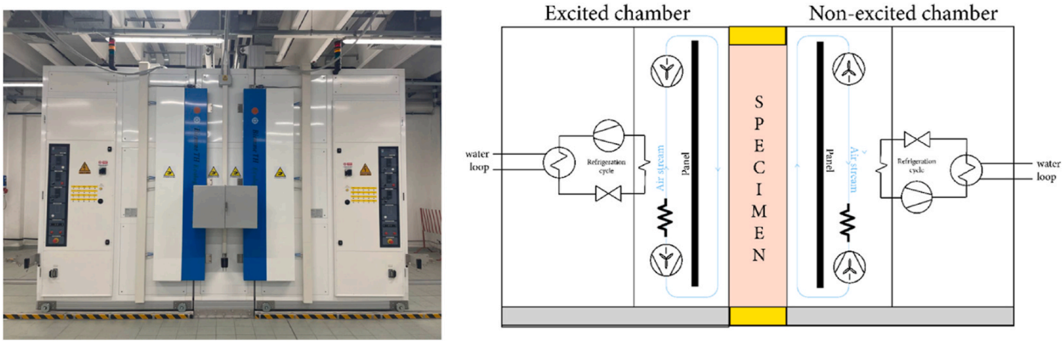

Fig. 3. The hot-box apparatus with the technical drawing of the system's components.

- 1 Data Logger (*Keysight* Model DAQ970A) with accuracy on the voltage measurement equal to ± 0.011% (range = 100 mV). Accuracy on the electrical resistance measurement equal to ± 0.012% (range = 100 Ω).
- 2 calibrated heat flux sensors HF-30S (*EKO Instruments*) of dimensions 30 cm × 30 cm x 0.05 cm for the measure of the heat flux across the measuring section of the wall. Sensor's sensitivity equal to 100 μV W^{-1} m^2. The ultra-light and thin thickness allow a more accurate measure with a low disturbance.

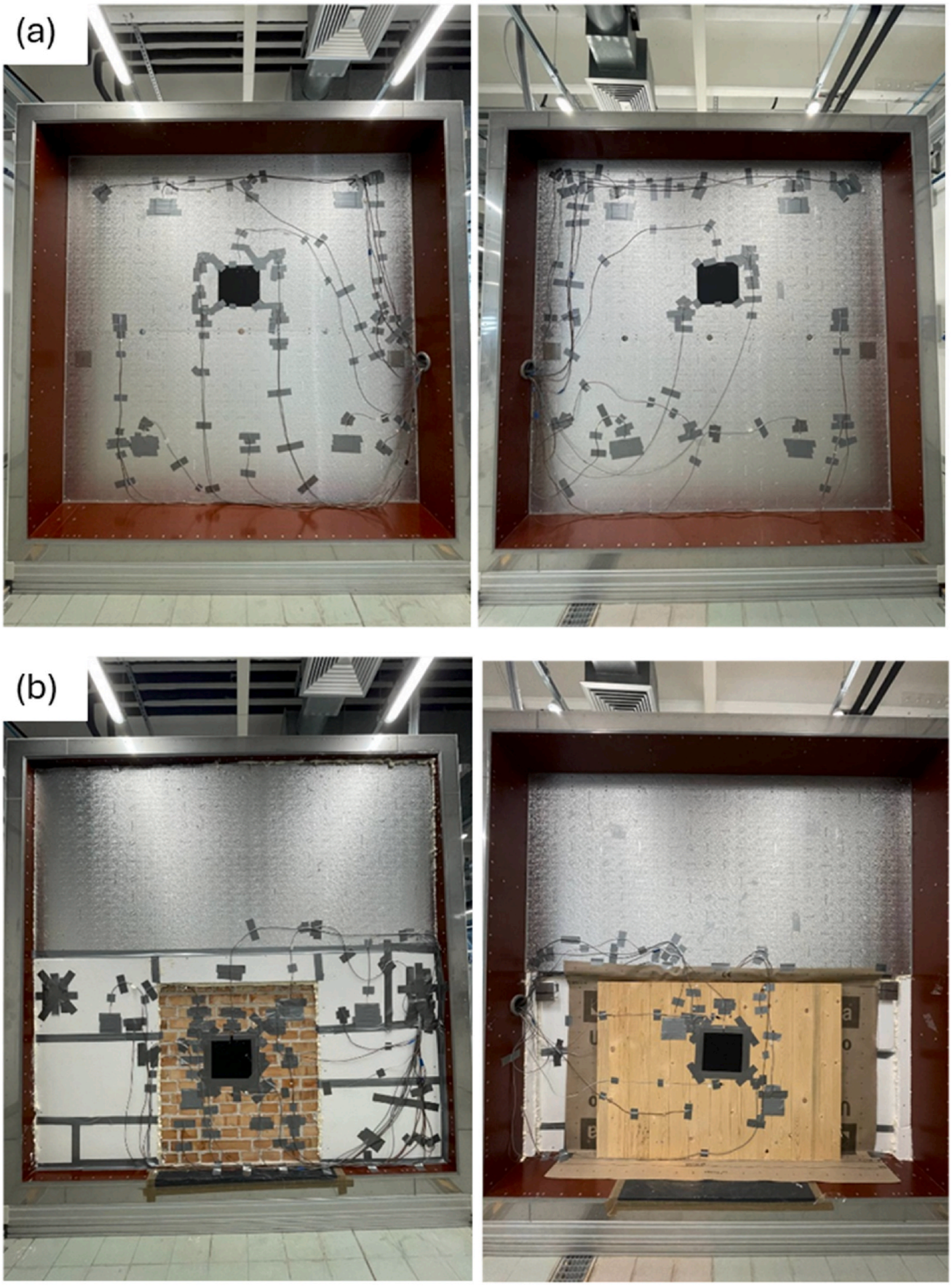

Fig. 4. Sensors installed on the non-excited side (left) and on the excited side (right) for the LW (a) and MW (b) cases.

- 6 Platinum Resistance Thermometers, particularly Pt100 surface contact probe, for the acquisition of the surface temperature in the measuring section. Accuracy equal to ±0.23 K (95% confidence level, coverage factor k = 1.96).
- 16 T-type thermocouples installed on the two surfaces to control the temperature homogeneity. Accuracy equal to ±1.07 °C (95% confidence level, coverage factor k = 1.96).
- 8 calibrated heat flux sensors HF-10S (*EKO Instruments*) of dimensions 10 cm × 10 cm x 0.05 cm were installed in the guard area as a verification for heat flux homogeneity during the test. Sensor's sensitivity equal to 10 μV W^{-1} m^2.

Fig. 4 shows the analysed wall with the sensors installed on both surfaces. Heat flux was measured simultaneously on both the excited and non-excited sides of the wall using calibrated heat flux sensors, enabling the independent evaluation of dynamic thermal transmittance from each surface, which is particularly relevant for high-inertia walls. All sensors were either provided with a calibration certificate, e.g., for the heat flux meters, or previously calibrated with a thermostatic bath (Hart Scientific Model 7025) over the temperature range which was supposed to be used. Heat flux meters and temperature sensors were installed on the surface of the wall with high conductive silicone paste and a tape with emissivity close to the one of the surface's walls. All recorded data was transferred to the external PC through LAN communication. The sampling time was set equal to 1 min.

To ensure full reproducibility of the experimental campaign, the testing procedure followed a structured sequence. After installation in the hot-box frame, each specimen was conditioned under laboratory-controlled temperature until thermal stabilization was achieved at the reference temperature $\overline{T}$. Prior to excitation, both chambers were maintained at this same temperature in order to establish uniform initial conditions across the wall section. Subsequently, Segment 1 was performed, consisting of the response-factor-based test described in Section 2.1. A triangular temperature excitation with predefined amplitude and duration was applied on the selected side, while all signals were continuously recorded with a sampling interval of 1 min. The completion of Segment 1 was identified by monitoring the reduction of the non-excited heat flux signal as it returned to zero. Heat flux signals measured on both the excited and non-excited sides were fitted according to Eqs. (1) and (2), allowing the dynamic U-value to be estimated. Segment 2, aimed at determining periodic thermal properties, was then initiated. This segment could begin immediately after Segment 1, as the wall temperature returned to $\overline{T}$, which also corresponds to the mean value of the sinusoidal excitation imposed during the periodic test. The sinusoidal temperature forcing was applied until a stabilized periodic regime was verified by comparing successive cycles, and the thermal parameters were estimated according to the equations reported in Section 2.2. Finally, to verify the U-value obtained from Segment 1, a steady-state reference test was conducted by imposing a constant temperature difference of 20 K between the chambers. Steady-state conditions were confirmed based on the stabilization of surface temperatures and heat flux over a defined time window. Measurement uncertainty for the periodic thermal properties and U-values was evaluated following the error propagation methodology described in Ref. [45]. The expanded uncertainty (95% confidence level, k = 1.96) of each directly measured quantity was first determined based either on sensor technical specifications (type B) or on statistical analysis of repeated measurements (type A). These uncertainties were subsequently propagated through the analytical expressions defining the computed thermal parameters, assuming independent variables.

3. Results and discussion

3.1. Simulated tests

An initial validation of the proposed method is carried out through a simulated test and is subsequently discussed by analysing in detail the results of the two test segments.

3.1.1. Segment 1: response factors test procedure

Segment 1 is designed for the determination of the U-value. To this end, a benchmark case was developed using finite element simulation under steady-state conditions. The transmittances were calculated through Eqs. (3) and (4) starting from the RF determined by FEM solutions.

The benchmark thermal transmittances are equal to 0.202 W m^{-2} K^{-1} for the LW and 0.733 W m^{-2} K^{-1} for the MW, respectively. Table 2 reports results of dynamic thermal transmittance ($U_{dyn,X}$ and $U_{dyn,Y}$) for two wall types, considering the application of the temperature pulse either at the internal or external side of the wall. The percentage deviation $\Delta_{benchmark}$ from the benchmark is reported, as well. Due to the symmetry, the application of the pulse on the inner side and on the outer side of the LW are equivalent. The numerical method closely reproduces the benchmark values. The $U_{dyn,X}$ is 0.204 W m^{-2} K^{-1} for LW which corresponds to a deviation of approximately +1.0% from the benchmark. For the MW wall, the $U_{dyn,X}$ is 0.737 W m^{-2} K^{-1} (pulse on the external side), matching the benchmark exactly. Differences between $U_{dyn,X}$ and $U_{dyn,y}$ stay below 1.6% for both walls highlighting the correctness of the calculation procedure.

Table 2
$U_{dyn,X}$ and $U_{dyn,Y}$ evaluated in the simulated test for the two samples.

Wall	Method	Temperature side	$U_{dyn,X}$ (W m^{-2} K^{-1})	$U_{dyn,Y}$ (W m^{-2} K^{-1})	$\Delta_{benchmark}$ (%)	
LW	Numerical	External/internal	0.204	0.202	+1.0%	0.0%
MW	Numerical	External	0.733	0.737	0.0%	+0.5%
		Internal	0.730	0.732	−0.4%	−0.1%

3.1.2. Segment 2: periodic test procedure

The numerical results confirm the expected influence of thermal mass on periodic thermal behavior. The LW shows a relatively high periodic thermal transmittance ($Y_{ie} = 0.193$ W m^{-2} K^{-1}), short time lag ($\Delta\tau_{ie} = 1.58$ h), and high decrement factor ($f = 0.929$), indicating a minimal shift and dampening of the external temperature solicitation. This reflects the low thermal storage capacity and limited delay in thermal response, typical of lightweight constructions. In contrast, the MW displays a lower periodic transmittance ($Y_{ie} = 0.137$ W m^{-2} K^{-1}), a significantly longer time lag ($\Delta\tau_{ie} = 10.95$ h), and a much lower decrement factor ($f = 0.196$). These values highlight the wall's ability to delay and attenuate the heat flux, due to its high thermal conductance, confirming the effectiveness of heavyweight constructions in reducing peak of heat flux under periodic thermal loads, such as daily solar gains. These results are consistent with previously published numerical and analytical values for wall assemblies with comparable thermal resistance and thermal mass, confirming that the model captures the expected mass-dependent periodic thermal response [36].

3.2. Experimental tests

A series of experiments were carried out to further validate the proposed methodology framework, with the aim of confirming its reliability for practical applications, while significantly reducing the time and energy costs typically associated with full-scale thermal testing.

3.2.1. Segment 1: response factors test procedure

Common test procedures for the assessment of the U-value of walls according to the standards [16,17] usually require a steady temperature gradient across the sample. By adopting standard procedure, a steady-state U-value equal to 0.202 W m^{-2} K^{-1} ±3.5% was obtained for the LW wall after 72 h. The U-value of the MW resulted equal to 0.719 W m^{-2} K^{-1} ± 4.7% after 216 h test in agreement with the higher thermal mass of the wall and the longer stabilization period. The uncertainties related to the steady-state thermal transmittance were assessed by adopting the theory of uncertainty in measurement [45] yielding to Eq. (15):

$$u_U = \sqrt{\frac{1}{\Delta T^2} \cdot \left[\varepsilon_{\dot{q}_i}^2 + \left(\varepsilon_{\Delta T}^2 \cdot \frac{\dot{q}_i^2}{\Delta T^2}\right)\right]} \tag{15}$$

where ΔT (K) is the temperature difference across the sample calculated by using average values, $\dot{q}_i$ (W m^{-2}) is the internal surface heat flux taken as average value over the stabilized period, and $\varepsilon_{\Delta T}$ (K) and $\varepsilon_{\dot{q}_i}$ (W m^{-2}) are the uncertainties related to the temperature difference and the one of the measured internal surface heat flux equal to 0.34 K and 0.12 W m^{-2}, respectively. The temperature difference uncertainty $\varepsilon_{\Delta T}$ was derived from the calibration accuracy of the platinum resistance probes (Type B uncertainty), while the uncertainty associated with the heat flux signal $\varepsilon_{\dot{q}_i}$ was estimated from the statistical variability of the stabilized measurements (Type An uncertainty) because of no sensor's accuracy present in the datasheet. These quantities represent random measurement uncertainty associated with the instrumentation and data acquisition system.

These U values were taken as a reference for the validation of the new experimental approach, in which transmittance is determined through segment 1 of the test procedure. For the lightweight wall, due to the layer symmetry, only one test was run applying the triangular profile at the external side. On the contrary, for the MW case, two tests were conducted to investigate both thermal responses when applying the triangular profile either at the masonry side or the CLT surface. The temperature magnitude adopted for the LW was set equal to 10 K, while for the more massive wall equal to 20 K in order to increase the signal-to-noise ratio of the measured heat flux at the opposite side of the solicitation. Such parameters were obtained by the simulated tests for optimizing the signal-to-noise ratio and the energy consumption of the hot-box apparatus. Table 3 reports results of dynamic thermal transmittance ($U_{dyn,X}$ and $U_{dyn,y}$) for two wall types during the experimental validation.

The comparison between steady-state and dynamic transmittance values for the LW wall shows very good agreement. The reference steady-state U-value is $U = 0.202$ W m^{-2} K^{-1}, while the dynamic values are $U_{dyn,X} = 0.210$ and $U_{dyn,Y} = 0.194$ W m^{-2} K^{-1}, corresponding to deviations of ±4.0% in line with the uncertainty of the steady state measurement. These values not only fall within a narrow range around the steady-state benchmark but also lie widely within the ±7% uncertainty of the U_{dyn} interval estimated with Eq. (16) according to the measurement's uncertainty theory [45].

$$u_{U_{dyn}} = \frac{0.07}{1 - \frac{\sum \dot{q}}{k}} \tag{15}$$

where 0.07 represents the heat flux uncertainty measurement equal to 7% [46], while the summation of the heat flux is taken either the excited or non-excited term reported in Eqs. (3) and (4) according to the considered side, and the constant k represents the heat flux

Table 3
$U_{dyn,X}$ and $U_{dyn,Y}$ evaluated in the experimental test for the two samples.

Wall	Method	Temperature side	$U_{dyn,X}$ (W m^{-2} K^{-1})	$U_{dyn,Y}$ (W m^{-2} K^{-1})	$\Delta_{benchmark}$ (%)	
LW	Experimental	External/Internal	0.210	0.194	+4.0	−4.0
MW	Experimental	External	1.117	0.415	+55.3	−42.3
		Internal	1.414	0.690	+96.7	−4.0

meter zero-offset equal to 0.1 W m^{-2}. Since the summation term results higher than the offset for both walls, the uncertainty of the dynamic U-value yields to the heat flux uncertainty. Small difference between $U_{dyn,X}$ and $U_{dyn,Y}$ remains below the typical measurement uncertainty and is therefore considered negligible (+1.60%). This overall consistency confirms that both values are in good agreement with the reference U-value, validating the methodology for lightweight assemblies.

For the MW wall, the comparison highlights more critical deviations due to its higher thermal mass. The reference U-value is 0.719 W m^{-2} K^{-1}, yet dynamic results differ substantially depending on the side and direction considered. When the temperature profile is applied at the external side (CLT surface), $U_{dyn,X}$ results in 1.117 W m^{-2} K^{-1}, showing a deviation of +55.4%, while when applied at the internal side (masonry wall), $U_{dyn,X}$ increases further to 1.414 W m^{-2} K^{-1} (+96.7%). It should be noted that these deviations are significantly larger than the estimated experimental uncertainty and therefore cannot be attributed solely to measurement noise. This indicates that the discrepancy is associated with other mechanisms than a random experimental error. These large deviations can be attributed primarily to the heat fluxes measured on the excited side, where the high imposed ΔT induces surface overheating, altering the thermal properties of the materials and especially the heat transfer by radiation inside the cavities of the porous materials namely timber and hollow brick. Temperature variations are known to influence the apparent thermal conductivity of porous materials due to intrinsic material property changes and enhanced radiative heat transfer within internal cavities [10]. In addition to this, the elevated temperature gradient also promotes mass transport phenomena: moisture present in hygroscopic materials can evaporate and migrate in vapor phase toward the cooler regions of the assembly, where it may recondense. This vapor migration is associated with an additional latent heat transfer, which increases the apparent thermal conductivity of the layer and, consequently, the overall thermal transmittance. Although moisture redistribution was not directly measured in the present study and no coupled hygrothermal simulations were performed, the combined temperature-dependent and moisture-dependent variability of thermal conductivity represents a physically plausible mechanism contributing to the observed overestimation of the dynamic U-value when the heat flux is measured on the excited side.

Conversely, the non-excited U-value obtained when the temperature solicitation is applied at the external side (CLT layer) equals 0.415 W m^{-2} K^{-1}, underestimating the reference U-value by −42.3%. When the dynamic U-value is derived from the heat flux measured on the non-excited side, a different behavior is observed. Since this surface is maintained at a constant temperature during the excitation, temperature and moisture-related effects are expected to be significantly reduced. In this configuration, the dominant source of deviation is associated with truncation of the transient response. In fact, this behavior can be linked to truncation errors in the dynamic response, especially when test duration is insufficient to capture long-term heat propagation (Fig. 5). Among all dynamic values for the massive wall, $U_{dyn,Y}$ = 0.690 W m^{-2} K^{-1} (solicitation at masonry side) is the only one closely aligned with the reference U, showing a deviation of just −4.0%. This indicates that measurements taken on the non-excited side, when the temperature profile is applied to the masonry layer, benefit from a faster and more stable thermal response, less affected by truncation and mass transport

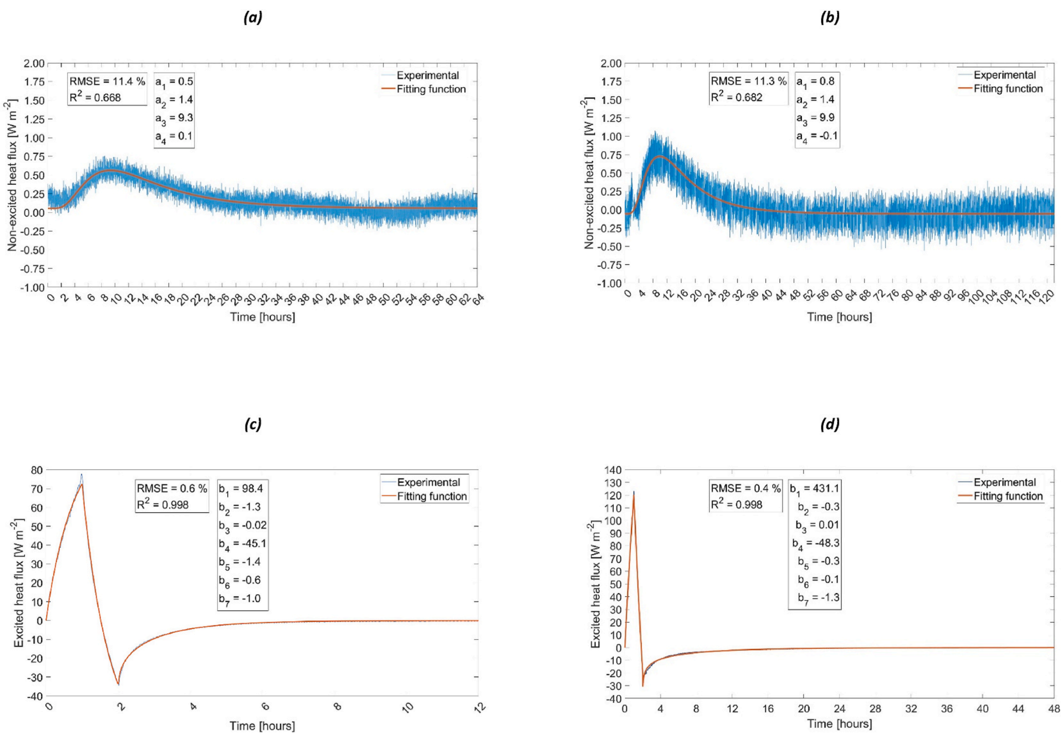

Fig. 5. Experimental heat fluxes and their fitting function in MW when pulse is applied the external side (a-c) and on the internal side (b-d). The excited heat flux trends were truncated once they reached zero for graphical purposes. Test durations are the same of the non-excited heat flux trends.

effects. Such value also falls within the 7% uncertainty interval established by Eq. (15), supporting the reliability of the methodology. Additionally, the relative agreement between $U_{dyn,X}$ and $U_{dyn,Y}$ in the LW case, and partially in the MW case, further confirms the method's robustness, provided that the test parameters are properly controlled. From a methodological perspective, it is worth noting that the reduced duration of the dynamic test with respect to the steady-state ones does not inherently increase the uncertainty of the U-value determination. While steady-state uncertainty is mainly governed by the stability of the imposed temperature difference and long-term averaging, the uncertainty associated with the dynamic approach is dominated by heat flux measurement accuracy. When test duration and excitation magnitude are properly selected, the resulting uncertainty levels are comparable to those obtained from steady-state tests. However, insufficient test duration may lead to truncation of the thermal response, particularly for high-inertia walls, introducing systematic deviations rather than increased random uncertainty. Such deviations are therefore interpreted as systematic methodological bias related to incomplete integration of the transient heat flux signal, rather than as random measurement uncertainty accounted in the propagation analysis. Truncation errors arise from the experimental procedure when the heat-flux signal is not allowed to fully decay to zero and are therefore independent of the random uncertainty associated with the measurement instrumentation. This interpretation is supported by the case in which the excitation is applied on the masonry side and the heat flux is evaluated on the non-excited surface, where the dynamic U-value deviation falls within the random uncertainty interval of the steady-state reference value. On the contrary, when the excitation is applied at the timber side, which exhibits higher global thermal inertia, the non-excited heat flux requires a longer time to return to zero and truncation errors may arise. In fact, this distinction explains the different uncertainty behavior observed between lightweight and massive walls, where the latter are more sensitive to test duration due to longer thermal response times. In addition, the tests on the MW wall show that the magnitude of applied solicitation is the key parameter for ensuring measurement accuracy. To guarantee a high signal to noise ratio, the intensity of the pulse must be maximized. On the other hand, however, particularly in hygroscopic and porous materials, this may lead to errors associated with the local alteration of material properties, and especially of the apparent thermal conductivity.

3.2.2. Segment 2: periodic test procedure

Table 4 reports results of the experimental periodic thermal parameters computed adopting the original signal in terms of temperature and heat flux, as well as the filtered one through Fast Fourier Transform (FFT) for both analysed walls.

For the lightweight wall, both results from the original signal and those filtered via FFT, are in strong accordance with the numerical outcomes. The periodic thermal transmittance obtained experimentally was equal to 0.195 W m^{-2} K^{-1} (±14.0%), slightly higher than the numerical value of 0.193 W m^{-2} K^{-1}, while the FFT-processed signal yielded 0.185 W m^{-2} K^{-1}. Similarly, the time-shift of 1.53 h (±1.2%) for the raw data and 1.33 h after FFT filtering showed extremely good agreement with the numerically predicted 1.58 h, especially for the raw data with deviations up to −3%. The decrement factor (f) follows the same trend: experimental values of 0.934 (±13.6%) and 0.899 (FFT) are very close to the simulated result of 0.929 (maximum deviations are lower than −3%). These consistent values indicate that the LW exhibits minimal shift and dampening of external thermal forcing, as expected from a structure with low thermal mass and storage capacity. In contrast, the MW displays remarkable different behavior, reflecting the effect of its higher thermal inertia. The periodic thermal transmittance drops significantly, with experimental values of 0.152 W m^{-2} K^{-1} (±14.0%) from the original signal and 0.120 W m^{-2} K^{-1} with FFT filtering procedure (in good agreement with numerical result: 0.137 W m^{-2} K^{-1}, with maximum deviation equal to −12%). The time-shift increases substantially to 10.95 h in the numerical model, which closely matches the FFT-experimental value of 10.12 h, and slightly less with the original signal at 9.09 h (±0.2%). The decrement factor also reflects the increased capacity to buffer thermal fluctuations: numerical f-value equals 0.196, while experimental values are 0.194 (±24.2%) and 0.155 (FFT).

The differences between measured and simulated values remained within the estimated uncertainty range of the experimental measurements, supporting the validity of the experimental method linking measured quantities to periodic thermal properties. Obtained results support the idea that thermal mass plays a critical role in the dynamic thermal performance of building components, particularly under periodic boundary conditions such as daily temperature profiles. The filtering of experimental data through FFT also proves to be an effective tool for improving the accuracy of the periodic thermal characterizations, especially in the evaluation of the time-shift.

4. Discussion

4.1. Potential time and energy savings from the response factors test procedure

Findings related to Segment 1, based on the Response Factors test procedure, demonstrate the applicability of the proposed methodology to the two analysed wall typologies. For the lightweight wall, the procedure provided stable results within the test

Table 4
Experimental periodic thermal parameters adopting either the original and the filtered signal.

Parameter	LW Original signal	LW FFT	MW Original signal	MW FFT
Y_{ie} (W m^{-2} K^{-1})	0.195 (±14.0%)	0.185	0.152 (±14.0%)	0.120
$\Delta\tau_{ie}$ (h)	1.53 (±1.2%)	1.33	9.09 (±0.2%)	10.12
f (−)	0.934 (±13.6%)	0.899	0.194 (±24.2%)	0.155

configurations investigated. For the massive wall, the procedure remained applicable, although increased attention was required, as test durations must be sufficiently long to avoid truncation, and input temperature magnitudes should be carefully adjusted, especially for porous materials whose apparent thermal conductivity can vary significantly with temperature. In addition to thermal inertia, the moisture behavior of hygroscopic materials in the MW wall may contribute to the deviations observed during the tests. Materials such as bricks, mortar, and timber are known to be hygroscopic and may exhibit coupled thermal and moisture-related effects when exposed to temperature gradients. In the present study, moisture transport was not explicitly investigated, and experimental boundary

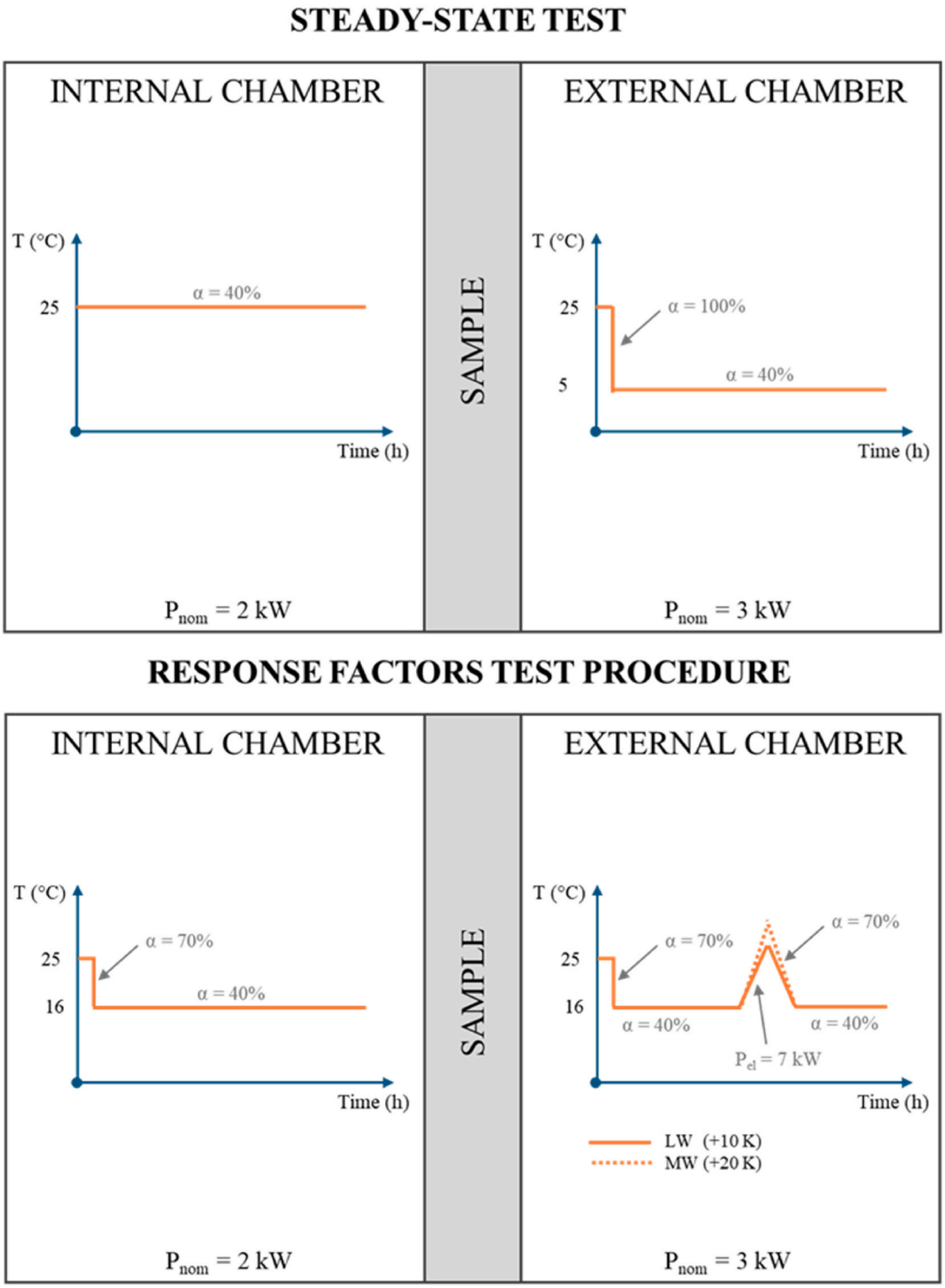

Fig. 6. Load profiles for the steady-state test and the response factors test in the hot-box apparatus.

conditions were designed to minimize vapor pressure gradients and moisture redistribution within the wall assemblies. However, based on previous experimental experience with masonry components, it cannot be excluded that limited residual moisture movements may still occur locally, even under controlled conditions. Such effects could introduce additional latent heat contributions, and lead to small deviations in the measured thermal response, particularly in dynamic tests where measured heat fluxes are small. While these effects were intentionally reduced in the experimental design, their potential influence should be considered, especially when a high-magnitude triangular excitation is locally applied to increase the heat-flux intensity. This aspect must be considered when interpreting the results and may be justify further investigation in future studies specifically addressing coupled heat and moisture transport.

The present results do not aim to demonstrate a general validity of the methodology for all wall typologies, nor to replace existing standardized hot-box procedures, but rather to discuss its performance and limitations under controlled laboratory conditions when applied to two representative cases with markedly different thermal resistance and thermal inertia. Further investigations involving walls with comparable thermal resistance and different inertia levels would be required to systematically map the applicability of the procedure across a broader range of construction solutions typical of specific regions or building stocks.

The methodology offers significant advantages in terms of time and energy savings. When testing lightweight walls, time reduction reaches up to −50% (passing from 72 h to 36 h), while for the MW case, considering the most reliable test configuration, time is reduced on average by a −21.3% moving from 216 h to 170 h. This has a direct effect on the energy consumption of the double climatic chamber involved in those experimental procedures which can be extremely energy-consuming. Fig. 6 represents the two procedures adopted to measure the U-value of the walls: one steady-state procedure and the periodic one. The internal chamber represents the non-excited one, while the external chamber is the so-called excited one. Considering the load profiles of the two chambers over time, their nominal electrical power absorptions P_{nom} and the corresponding load factors α along profiles, energy consumptions could be estimated for each test as reported in Table 5. Calculations included the power of the electrical resistances P_{el} equal to 3 kW per chamber and auxiliaries, as well. By running a dynamic test, the required energy is 86.9 kWh with respect to the steady-state one which is equal to 135.3 kWh, for the LW wall, with an energy and cost reduction of −35.8%. As regards the MW case, energy consumption passed from 525.3 kWh (steady-state) to 231.6 kWh (dynamic) with an energy and cost reduction −55.9%. These savings specifically refer to the U-value assessment, which is typically the most time and energy-consuming phase of hot-box testing. In addition, the Response Factors procedure provides a further indirect benefit at the experimental campaign level. Since the dynamic test concludes under stable thermal conditions close to the initial equilibrium state, the subsequent periodic test can be started without requiring a separate pre-conditioning phase. This sequential use of dynamic and periodic procedures contributes to a reduction of the overall testing time and associated energy consumption when both steady-state and periodic thermal properties are evaluated within a single experimental campaign.

5. Conclusions

This study presented a comprehensive experimental workflow for the rapid and subsequent assessment of both steady-state and periodic thermal properties of building envelope components using a hot-box facility. The combination of a triangular dynamic test and a sinusoidal periodic test within a controlled hot-box environment was applied to two representative wall assemblies with different thermal resistance and thermal inertia, enabling the determination of the U-value and periodic thermal parameters within a single experimental campaign. The Response Factors procedure test provided stable results for the lightweight wall within the investigated configurations, achieving U-values within approximately 4% deviation of the steady-state benchmark while reducing testing time and energy consumption by up to 50% and 34%, respectively. These results indicate that, for lightweight constructions, the dynamic procedure represents an effective and less energy-intensive alternative to conventional steady-state hot-box testing, increasing the overall efficiency of the single experimental campaign. For massive walls, the application of the methodology required increased attention to test duration and excitation magnitude to avoid truncation effects and local alterations of the material properties that could undermine the linearity of the problem and thus the accuracy of the results. When heat flux measurements on the non-excited side were considered and test parameters were optimized, the dynamic approach achieved U-values within approximately 4% of the reference. Deviations observed in some test configurations are attributed to a combination of thermal inertia and possible residual moisture-related effects, which were intentionally minimised but not explicitly modelled in this study. Results suggest that mass transport in walls with hygroscopic materials may contribute to deviations in the measured thermal response, leading to an overestimation of the thermal transmittance value. Such effects were not the focus of the present work and were intentionally limited through specimen conditioning and controlled boundary conditions but cannot be fully excluded based on previous experimental experience with masonry walls.

Regarding the main novelty of the presented work, the periodic test enabled the experimental determination of periodic thermal transmittance, decrement factor, and time shift, based on a measurement-based formulation linking experimental hot-box data to periodic thermal parameters. Differences between the lightweight and massive walls, where the latter showed significantly greater

Table 5
Energy consumptions for the steady-state and the response factors in kWh.

Procedure	LW	MW
Steady-state	135.3 kWh	525.3 kWh
Response Factors	86.9 kWh	231.6 kWh

time-shift and attenuation of the heat flux, highlighted the influence of thermal mass on the time-dependent performance. The application of FFT-based filtering improved the robustness of periodic parameter estimation under noisy experimental conditions. The proposed test framework enables a faster and less energy-intensive alternative to traditional steady-state tests without compromising the accuracy, particularly for U-value assessment, which is typically the most time and energy-consuming phase of hot-box testing. For the lightweight wall, an energy and cost reduction of 35.8% was achieved, while for the massive wall the reduction reached 55.9% under the analysed conditions. Such savings refer specifically to the dynamic U-value determination, however, causing advantages in test time to the overall combined procedure. However, for walls characterized by a higher thermal inertia and materials with thermal properties strongly depending on temperature, attention must be paid to boundary conditions, magnitude of the triangular temperature profile, and test duration to avoid over- or underestimation of the U-value.

The results presented do not establish a general validation of the methodology for all wall typologies, but rather illustrate its applicability, advantages, and limitations through two representative case studies. Further investigations involving wall assemblies with comparable thermal resistance and varying levels of thermal inertia would be required to systematically assess the range of applicability of the proposed framework and to develop a comprehensive testing roadmap. Nevertheless, when properly applied, this dual-test framework using dynamic and periodic tests within a single campaign, offers a promising path toward efficient, reliable, and comprehensive thermal characterization of building envelope systems, supporting both regulatory compliance and the design of energy-resilient buildings.

CRediT authorship contribution statement

Maja Danovska: Conceptualization, Data curation, Methodology, Software, Validation, Visualization, Writing – original draft. **Davide Cassol:** Conceptualization, Methodology, Writing – review & editing. **Ivan Giongo:** Writing – review & editing. **Alessandro Prada:** Conceptualization, Methodology, Writing – review & editing.

Declaration of competing interest

The authors declare that they have no known competing financial interests or personal relationships that could have appeared to influence the work reported in this paper.

Acknowledgments

The 2024-2026 ReLUIS-DPC project is gratefully acknowledged for the support given to the research.

Data availability

Data will be made available on request.

References

[1] Eurostat – European Commission, Energy statistics - an overview [Online]. Available: https://ec.europa.eu/eurostat/statistics-explained/index.php?title=Energy_statistics_-_an_overview#Final_energy_consumption, 2022.
[2] M. González-Torres, L. Pérez-Lombard, Juan F. Coronel, Ismael R. Maestre, Da Yan, A review on buildings energy information: trends, end-uses, fuels and drivers, Energy Rep. 8 (2022) 626–637, https://doi.org/10.1016/j.egyr.2021.11.280.
[3] European Parliament and Council of the European Union, Directive (EU) 2024/1275 of the European Parliament and of the council of 24 April 2024 on the energy performance of buildings (recast), Off. J. Eur. Union (2024). L 123, 12 May 2024.
[4] N. Bishara, G. Pernigotto, A. Prada, M. Baratieri, A. Gasparella, Experimental determination of the building envelope's dynamic thermal characteristics in consideration of hygrothermal modelling – assessment of methods and sources of uncertainty, Energy Build. 236 (2021) 110798, https://doi.org/10.1016/j.enbuild.2021.110798.
[5] Z. Shen, A.L. Brooks, Y. He, S.S. Shrestha, H. Zhou, Evaluating dynamic thermal performance of building envelope components using small-scale calibrated hot box tests, Energy Build. 251 (2021) 111342, https://doi.org/10.1016/j.enbuild.2021.111342.
[6] A. Prada, E. Bee, M. Grigiante, P. Baggio, On the optimal mix between lead-acid battery and thermal storage tank for PV and heat pump systems in high-performance buildings, Energy Proc. 140 (2017) 423–433, https://doi.org/10.1016/j.egypro.2017.11.154.
[7] M. Pinamonti, A. Prada, P. Baggio, Rule-based control strategy to increase photovoltaic self-consumption of a modulating heat pump using water storages and building mass activation, Energies 13 (23) (2020) 6282, https://doi.org/10.3390/en13236282.
[8] CEN European committee for Standardization, EN ISO 6946. Building Components and Building Elements — Thermal Resistance and Thermal Transmittance — Calculation Methods, 2018.
[9] CEN European committee for Standardization, EN ISO 13786. Prestazione Termica dei Componenti per Edilizia - Caratteristiche Termiche Dinamiche - Metodi di Calcolo, 2018.
[10] M. Danovska, G. Pernigotto, P. Baggio, A. Gasparella, Simulation uncertainty in heat transfer across timber building components in the Italia climates: the role of thermal conductivity, Energy Build. 268 (2021) 112190, https://doi.org/10.1016/j.enbuild.2022.112190.
[11] E. Lucchi, Thermal transmittance of historical brick masonries: a comparison among standards data, analytical calculation procedures, and in situ heat flow meter measurements, Energy Build. (2017), https://doi.org/10.1016/j.enbuild.2016.10.045.
[12] D. Majcen, L. Itard, H. Visscher, Actual and theoretical gas consumption in Dutch dwellings: what causes the differences? Energy Policy 61 (Supplement C) (2013) 460–471, https://doi.org/10.1016/j.enpol.2013.06.018.
[13] D. Majcen, L.C.M. Itard, H. Visscher, Theoretical vs actual energy consumption of labelled dwellings in the Netherlands: discrepancies and policy implications, Energy Policy 54 (2013) 125–136, https://doi.org/10.1016/j.enpol.2012.11.008.
[14] A. Rasooli, L. Itard, C.I. Ferreira, A response factor-based method for the rapid in-situ determination of wall's thermal resistance in existing buildings, Energy Build. 119 (Supplement C) (2016) 51–61, https://doi.org/10.1016/j.enbuild.2016.03.009.

[15] N. Soares, C. Martins, M. Gonçalves, P. Santos, L. Simões da Silva, J.J. Costa, Laboratory and in-situ non-destructive methods to evaluate the thermal transmittance and behavior of walls, windows, and construction elements with innovative materials: a review, Energy Build. 182 (2019) 88–110, https://doi.org/10.1016/j.enbuild.2018.10.021.
[16] CEN European committee for Standardization, EN ISO 8990, Thermal Insulation – Determination of steady-state Thermal Transmission Properties – Calibrated and Guarded Hot Box, 1996.
[17] CEN European committee for Standardization, EN ISO 1934. Thermal Performance of Buildings - Determination of Thermal Resistance by Hot Box Method Using Heat Flow Meter - Masonry, 2000.
[18] F. Asdrubali, G. Baldinelli, Thermal transmittance measurements with the hot box method: calibration, experimental procedures, and uncertainty analyses of three different approaches, Energy Build. 43 (2011) 1618–1626, https://doi.org/10.1016/j.enbuild.2011.03.005.
[19] G. Baldinelli, F. Bianchi, A.A. Lechowska, J.A. Schnotale, Dynamic thermal properties of building components: hot box experimental assessment under different solicitations, Energy Build. 168 (2018) 1–8, https://doi.org/10.1016/j.enbuild.2018.03.001.
[20] G. Pernigotto, A. Prada, F. Patuzzi, M. Baratieri, A. Gasparella, Characterization of the dynamic thermal properties of the opaque elements through experimental and numerical tests, Energy Proc. 78 (2015) 3234–3239, https://doi.org/10.1016/j.egypro.2015.11.786.
[21] J.M. Sala, A. Urresti, K. Martin, I. Flores, A. Apaolaza, Static and dynamic thermal characterisation of a hollow brick wall: tests and numerical analysis, Energy Build. 40 (2008) 1513–1520, https://doi.org/10.1016/j.enbuild.2008.02.011.
[22] K. Martin, I. Flores, C. Escudero, A. Apaolaza, J.M. Sala, Methodology for the calculation of response factors through experimental tests and validation with simulation, Energy Build. 42 (2010) 461–467, https://doi.org/10.1016/j.enbuild.2009.10.015.
[23] G. Mitalas, D.G. Stephenson, Room thermal response factors, ASHRAE Trans. 73 (1) (1967) 1–10.
[24] D.G. Stephenson, G.P. Mitalas, Cooling load calculations by the thermal response factor method, ASHRAE Trans. 73 (1967).
[25] G.P. Mitalas, D.G. Stephenson, Calculation of heat flows through walls and roofs, ASHRAE Trans. 74 (1968) 182–188.
[26] X.Q. Li, Y. Chen, J.D. Spitler, D. Fisher, Applicability of calculation methods for conduction transfer function of building constructions, Int. J. Therm. Sci. 48 (7) (2009) 1441–1451, https://doi.org/10.1016/j.ijthermalsci.2008.11.006.
[27] E. Bettanini, P.F. Brunello, Lezioni di Impianti Tecnici, vol. 2, CLEUP Editore, 1990.
[28] M.G. Davies, Building Heat Transfer, WILEY, 2004.
[29] D. Hittle, Response factors and conduction transfer functions. www.web.mit.edu, 1992.
[30] I.S. Iu, Experimental Validation of the Radiant Time Series Method for Cooling Load Calculations, M.S. thesis, Oklahoma State Univ., Stillwater, OK, USA, 2002.
[31] Y. Yang, T.V. Wu, A. Sempey, J.-C. Batsale, Short time non-destructive evaluation of thermal performances of building walls by studying transient heat transfer, Energy Build. 184 (2019) 141–151, https://doi.org/10.1016/j.enbuild.2018.12.002.
[32] L. Evangelisti, E. De Cristo, S. Monteleone, C. Guattari, P. Gori, D. Ambrosini, Development and validation of a non-contact method for U-value estimation in heritage and existing buildings, Results Eng. 47 (2025) 107276, https://doi.org/10.1016/j.rineng.2025.107276.
[33] W.H. Press, S.A. Teukolsky, W.T. Vetterling, B.P. Flannery, Numerical Recipes: the Art of Scientific Computing, third ed., Cambridge University Press, Cambridge (UK), 2007.
[34] MathWorks®. MATLAB®, *Fast Fourier Transform* Function, 2022. https://it.mathworks.com/help/matlab/ref/fft.html.
[35] M.D. Mittleman, Waves and the wave equation [PDF document], Retrieved from Lecture Notes Online Website, https://www.brown.edu/research/labs/mittleman/sites/brown.edu.research.labs.mittleman/files/uploads/lecture02_0.pdf.
[36] D. Cassol, M. Danovska, A. Prada, I. Giongo, Timber-based strategies for seismic collapse prevention and energy performance improvement in masonry buildings, Sustainability 16 (2024) 392, https://doi.org/10.3390/su16010392.
[37] Thermal properties retrieved from https://www.aipe.biz/mondo-eps/polistirene/caratteristiche/.
[38] Infobuild.it. (n.d.). DPL ISOTEC PARETE 25 [PDF]. Retrieved June 11, 2025, from https://www.infobuild.it/wp-content/uploads/DPL_ISOTEC_PARETE_25_web.pdf.
[39] Institute of Physics. (n.d.). Specific heat capacity. IOPSpark. Retrieved June 11, 2025, from https://spark.iop.org/specific-heat-capacity.
[40] Technical datasheet TASSULLO ARMIS Malta strutturale alleggerita a base di calce idraulica NHL 5, retrieved from, https://www.tassullo.it/.
[41] T.K.T. Wolterbeek, S.J.T. Hangx, The thermal properties of set Portland cements – a literature review in the context of CO_2 injection well integrity, J. CO2 Util. 70 (2023) 102302, https://doi.org/10.1016/j.jcou.2023.102302.
[42] Technical datasheet XLAM Dolomiti. https://www.xlamdolomiti.it/local/storage/uploadz/Schede_Tecniche_XLAM_Dolomiti.pdf.
[43] F. Nocera, A. Gagliano, M. Detommaso, Energy performance of cross-laminated timber panel (X-Lam) buildings: a case study, Mater. Manuf. Process. 5 (3) (2018) 175–182, https://doi.org/10.18280/mmep.050307.
[44] COMSOL Multiphysics® v. 3.5a. www.comsol.com. COMSOL AB, Stockholm, Sweden.
[45] J.V. Nicholas, D.R. White, Traceable Temperatures. an Introduction to Temperature Measurement and Calibration, second ed., Wiley, 2001.
[46] International Organization for Standardization, ISO 9869-1. Thermal Insulation — Building Elements — In-situ Measurement of Thermal Resistance and Thermal Transmittance — Part 1: Heat Flow Meter Method, 2015.